Linearization of CMOS Hot-electron Injectors for Self-powered Monitoring of Biomechanical Strain Variations

Liang Zhou, *Student Member, IEEE*, and Shantanu Chakrabartty, *Senior Member, IEEE*

***Abstract*—In our previous work we demonstrated that by eliminating regulation and rectification modules from the energy harvesting pathway, the minimum activation power of a piezoelectricity-driven hot-electron injector (p-HEI) can be reduced down to a few nanowatts. As a result the p-HEI device could be used for self-powered, in-vivo recording of biomechanical strain variations. However, for large magnitudes of input strain energy, the response of the modified p-HEI sensor was found to be quasi-linear with respect to the number of loading cycles, which made the calibration of the sensor difficult across a wide variety of biomedical applications. In this paper we propose a compensation circuit that is able to linearize the response of the p-HEI injector over a wide range of input power while maintaining a low activation threshold. The compensation circuit uses a combination of a storage capacitor and a non-linear resistor which produces a compressive input-output response required for linearization. Using prototypes fabricated in a 0.5-μm bulk CMOS process we validate the functionality of the injector and demonstrate that it can achieve a linear injection response for input power ranging from 5 nW to 1.5 μW.**

Keywords*—Self-powered Sensors, Piezo-Floating-gate, Hot-electron Injection, Signal Compression, Biomechanics, Health and Usage Monitoring.

I. Introduction

CONTINUOUS monitoring of variations in mechanical strain presents a significant challenge when the sensor is operating in an embedded and an implanted environment due to limitations on the size of the sensor and due to unavailability of a continuous and reliable energy source (e.g. solar or radio-frequency) [1], [2], [3], [4]. Self-powered sensors based on piezoelectricity driven hot-electron injectors (p-HEI) can overcome these limitations by scavenging its operational energy directly from the strain-variations without requiring any additional source of energy [5], [6], [7]. As a result these devices can continuously monitor and store the statistics of the mechanical strain variations without experiencing any loss of data. The stored statistics could then be retrieved offline, using a radio-frequency [8] or an ultrasonic interface [9]. However, the applicability of a p-HEI sensor to different biomedical applications is determined by the power harvested by the transducers which in turn is determined by the level of ambient strain-variations, the volume of the transducer and the transducer's material properties. Fig. 1 compares different levels of electrical power that can be harvested from strain-variations in different biomechanical structures (ranging from stents in blood-vessels to a knee-implant) and by using different types of piezoelectric material. For example, using a Rochelle salt crystal (with $d_{21} = 700$) as an energy transducer, approximately a few nanowatts of power can be harvested from strain-variations at the surface of a blood-vessel (feature size in μm). The harvested energy could be used to monitor the mechanical usage of a stent implanted in a vessel [10]. On the other end of the energy/size spectrum, a PZT-5H ceramic embedded inside a sports helmet could be used to harvest milliwatts of power and used for monitoring head-impacts in contact sports [11]. In all these diverse applications, a p-HEI sensor could sense, compute and store historical strain-level statistics which can then be used either for diagnosis or for predicting any impending mechanical failure. Example of usage statistics include the total duration for which the structure experienced strain-levels that exceeded a pre-determined threshold level [8].

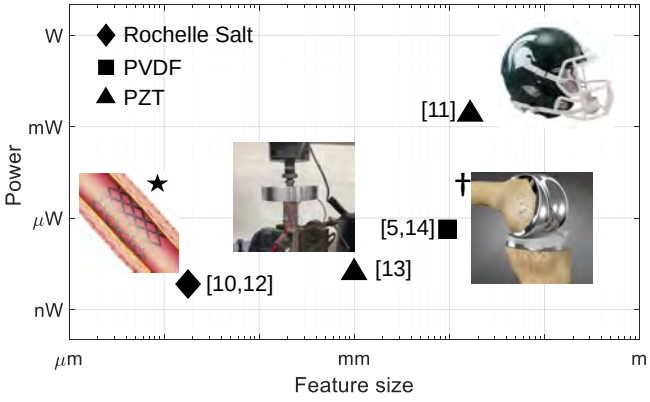

Fig. 1. Comparison of harvestable strain energy from different biomechanical structures and using different piezoelectric materials. (Image source: ⋆ from American Vein & Vascular Institute, † from Conformis).

In [13] we had proposed a p-HEI sensor that could operate at power levels as small as 5 nW. Compared to the previous generation of p-HEI sensors [6], [7], this was an order of magnitude improvement in energy-efficiency. As a result, the

This work was supported in part by research grants from the National Science Foundation (ECCS:1550096, CSR:1405273, CAREER:0954752). L. Zhou and S. Chakrabartty are with the Department of Computer Science and Engineering, Washington University in St. Louis, St. Louis, MO, 63130 USA. All correspondences regarding this paper should be addressed to Email: shantanu@wustl.edu

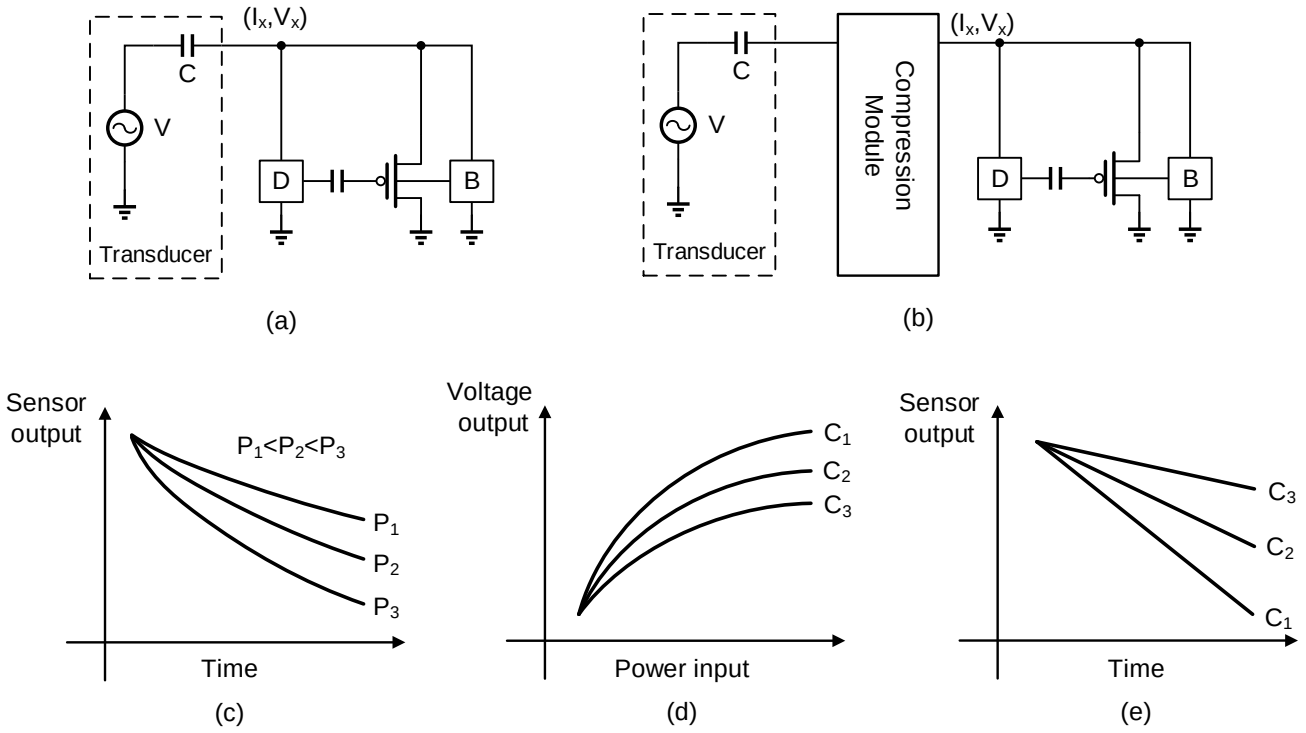

Fig. 2. Architecture of a p-IHEI sensor: (a) as reported in [13] without pre-compensation; and (b) proposed using a compensation circuit. The modules "D" and "B" in (a) denote biasing circuits for gate and bulk terminals. (c) Quasi-linear response of the injector shown in (a) as a function of mechanical loading; (d) desired response of the compensation circuit for different compression parameters C_i; and (e) Linearization effect by combining the responses in (c) and (d).

sensor could be miniaturized and could be used for implanted monitoring of strain-variations on the surface of a bone [13]. While the response of the injector was demonstrated to be linear for input power levels less than 50nW, its response become quasi-linear as the level of input power increased. This obviates the use of the technique for statistical monitoring of strain-levels in a range of applications shown in Fig. 1, where the harvestable power could vary from 1 nW to 1 mW. Addressing this limitation and extending the linear operating range is the main focus of this paper.

Fig. 2 shows the schematic of the p-HEI sensor circuit that was reported in [13]. A piezoelectric transducer operating in strain-mode has been modeled by its low-frequency equivalent circuit which directly drives the input of a floating-gate transistor. By eliminating the biasing and regulation circuitry from the direct signal path and by coupling the physics of piezoelectric energy transduction with the dynamics of hot-electron injection on the floating-gate transistor, the circuit is able to reduce its activation energy. A typical response of such injector as reported in [13] is illustrated in Fig. 2(c), where each curve corresponds to a different magnitude of input power. The response is quasi-linear with respect to time and the degree of non-linearity increases with magnitude of the input power. In this paper, we propose a compensation circuit with an input-output response as illustrated in Fig. 2(d). The objective will be to combine the injector response shown in Fig. 2(c) with the compressive response shown in Fig. 2(d) to obtain a linearized response shown in Fig. 2(e) using the compressive response to pre-compensate and linearize the p-HEI injector reported in [13].

The paper is organized as follows: Section II presents a mathematical model describing the operation of the proposed p-HEI injector, followed by Section III which presents system implementation and measurement results obtained from fabricated prototypes of the injector. Section IV concludes the paper with a discussion on the functionality of the proposed injector.

II. Mathematical Model of Compressive Low-power Injector

In a p-HEI sensor, the flow of electrons generated by a piezoelectric transducer as a result of a mechanical loading event is used to generate hot-electrons in the channel of a MOSFET transistor. Some of the hot-electrons generated in the channel surmount the gate-oxide energy barrier and manifest themselves as injection or gate current. If the gate terminal is terminated only by a capacitive load (also called floating-gate), any charge that is injected into the gate cannot leak out and results in a permanent change in the floating-gate voltage. This change in voltage is measured and then can be used to infer the statistics of the mechanical excitation. In this paper we introduce a compressive response circuit to modulate the interface between the piezoelectric transducer and the floating-gate transistor. An equivalent circuit model combining the

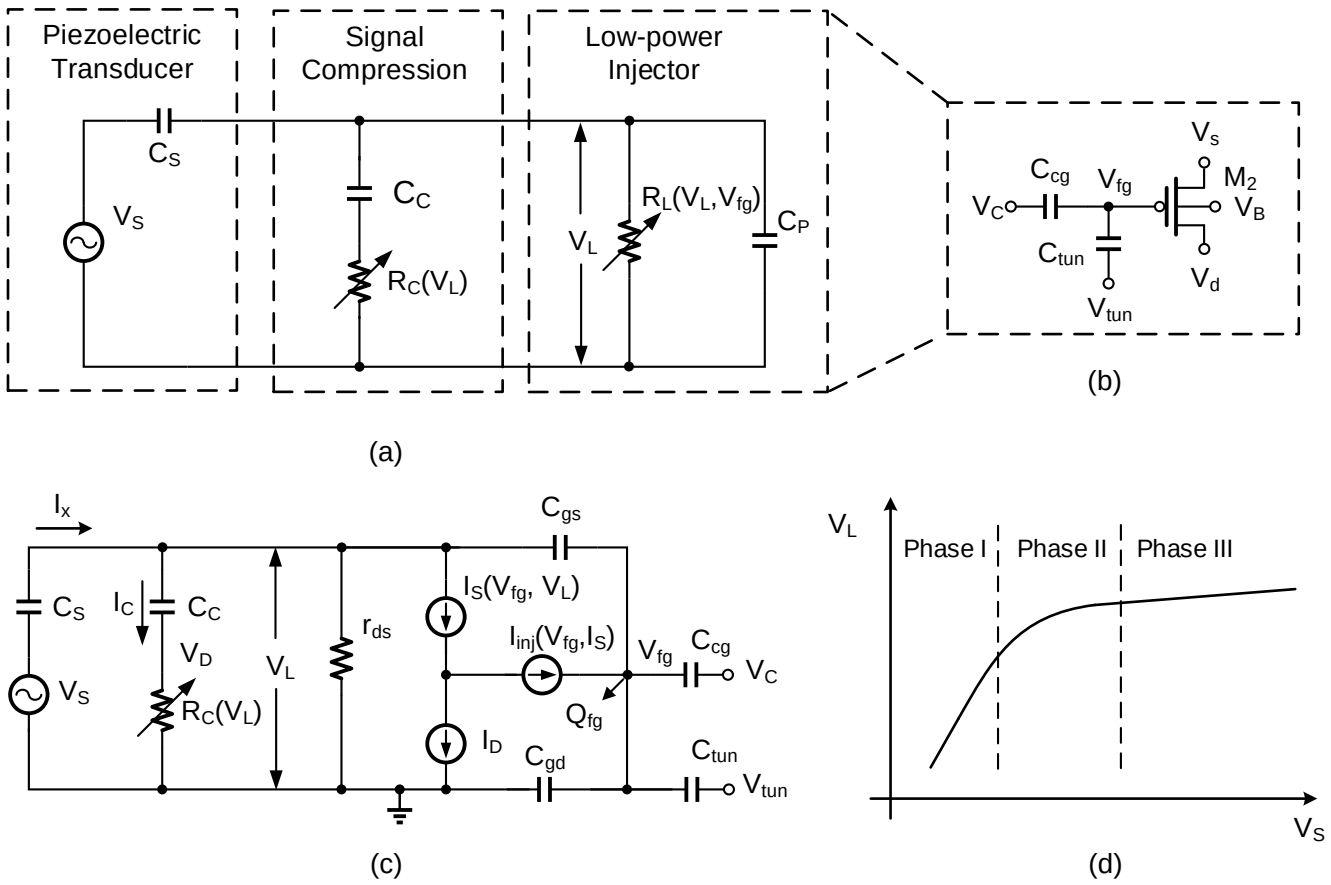

Fig. 3. Operation of the proposed p-IHEI sensor:(a) Simplified circuit of the system, (b) core circuit of the injector, (c) small-signal equivalent circuit of the sensor and (d) different phases of operation induced by the compression module.

model of a piezoelectric transducer, the compressive response circuit and the equivalent circuit of a floating-gate pMOS transistor is shown in Fig. 3. A piezoelectric transducer operating in strain-mode (non-resonance mode) is modeled as a series connection of voltage source and a capacitor [15]. The voltage source V_S models the electrical signal transduced by the strain variations and the capacitor C_S models the mechanical stiffness of the transducer. Both these variables are a function of the dimensions, the material properties and the mechanical configuration of the piezoelectric transducer. For a cantilever configuration of a transducer with dimensions $w \times l \times h$, the open-source voltage (V_S) generated can be expressed in terms of the mechanical force (F) perpendicular along the length as [15]:

$$V_S = \frac{F}{w} g_{31} = S(t) Y^E h g_{31} = \frac{S(t) Y^E d_{31} h}{\epsilon_p} \tag{1}$$

where g_{31} and d_{31} are piezoelectric constants, $S(t)$ is the time-varying mechanical strain, Y^E is the short circuit elastic modulus and ϵ_p is the electrical permittivity of the material. The capacitance in the equivalent circuit model is given by

$$C_S = \epsilon_p \frac{w \times l}{h} \tag{2}$$

The gate injection current I_{inj} is based on a model for hot-electron generation in a floating-gate transistor [7] relating the injection current I_{inj} to the terminal voltage V_L and the transistor source current I_S. This is expressed as [16]:

$$I_{inj} = -\beta I_S \exp(\frac{V_L}{V_{inj}}) \tag{3}$$

where β and V_{inj} are injection parameters that are a function of the transistor size and process parameters. When the source-to-drain voltage is larger than 200 mV, the channel current of a PMOS floating-gate transistor biased in weak-inversion region can be expressed in terms of its source voltage V_L, floating-gate voltage V_{fg} as [17]

$$I_S = I_0 \exp(\frac{-V_{fg}}{\kappa U_T}) \exp(\frac{V_L}{U_T}) \tag{4}$$

where I_0 is the characteristic current which is a function of process parameters, U_T is thermal voltage (≈26 mV at 300 K)

and κ is the gate efficiency factor. Here we assume the bulk V_B is connected to the source terminal. The transducer driving current I_x flowing through the source capacitance C_S can be expressed as:

$$I_x = Cs\frac{dV_S - dV_L}{dt} \tag{5}$$

By exploiting the small signal model we have

$$I_C = \frac{V_D}{R_C} \tag{6}$$

Notice that I_C charges and discharges C_c, we have

$$I_C = C_C\frac{dV_L - dV_D}{dt} \tag{7}$$

Since the injection current is relatively small, we have

$$I_x = I_C + \frac{V_L}{r_{ds}} + I_S + C_{gs}\frac{dV_L}{dt} \tag{8}$$

The change in floating-gate charge due to the injection current I_{inj} can be expressed by the following first order differential equation:

$$C_T\frac{dV_{fg}}{dt} = I_{inj} \tag{9}$$

where $C_T = C_{cg}+C_{tun}+C_{gs}$ is the total capacitance with C_{cg} being the gate-coupling capacitor, C_{tun} being the tunneling capacitor and C_{gs} being the gate-to-source capacitance. Given the form of V_S, the dependence of V_{fg} with respect to t can be derived by solving the differential equations 1-9. However, coupled form of the differential equations makes it difficult to derive a closed-form dependence of V_{fg} with respect to t. Instead we evaluate the response of the equivalent circuit for two boundary conditions and then extrapolate between the two responses.

The first boundary condition occurs when the magnitude of the input signal is small enough that $R_C(V_L) \approx \infty$. This is depicted by phase I in Fig. 3(d) where the piezo-capacitance C_S and the parasitic capacitance of the injector C_P act as a voltage divider. V_L and V_S are related as

$$\Delta V_L \approx \frac{C_S}{C_S + C_P}\Delta V_S \tag{10}$$

Note that since $C_P \ll C_S$, $\Delta V_L \approx \Delta V_S$, and the response of V_L follows the changes of V_S.

The other boundary condition occurs when the magnitude of the input signal is large enough that $R_C(V_L) \approx 0$ and is depicted by phase III in Fig. 3(d). During this condition V_L and V_S are related as

$$\Delta V_L = \frac{C_S}{C_S + C_C}\Delta V_S \tag{11}$$

If we choose $C_C \gg C_S$, then the input-output response is $\Delta V_L \approx 0$ as illustrated in the phase III of Fig. 3(d). In the intermediate phase II the response can be extrapolated between phase I and phase III as

$$\Delta V_L = \left(\gamma\frac{C_S}{C_S + C_P} + \theta\frac{C_S}{C_S + C_C}\right)\Delta V_S \tag{12}$$

where γ and θ are weighting coefficients that can be adjusted to achieve the desired pre-compensation.

III. System Implementation and Measurement Results

A. Circuit implementation of the Injector

Fig. 4 shows the complete schematic of the proposed injector implemented in a standard bulk CMOS process. The design is fully differential as a result of which the circuit can be directly driven by a piezoelectric transducer without any rectification. P_1 is the floating-gate transistor and C_{fg} is the control-gate that couples the control-gate voltage V_{cg} with the floating-gate voltage V_{fg}. C_{tun} is a junction capacitance used for tunneling electrons out of the floating-gate according to the procedure described in our previous papers [6] to program the initial charge on the FG node. The cross-coupled transistor pair P_2 and P_3 ensures that the substrate of P_1 is maintained at the highest potential irrespective of the polarity of the input voltages V_{in1} and V_{in2}. The diode chain D_1 to D_{14} serve three functions: (a) they limit the input voltage amplitude $|V_{in1} - V_{in2}|$ to be within a compliant operating range; (b) they generate the bias for the control-gate voltage $V_{cg} \approx V_{dio}$, where V_{dio} is the voltage drop on a p-n diode (D_7 and D_{14} in Fig. 4); and (c) they modulate the gate voltages of transistors M_{C1} and M_{C2} based on the difference in the input voltages V_{in1} and V_{in2}. Thus, M_{C1}, C_{C1} and M_{C2}, C_{C2} implements a differential version of R_C and C_C shown in Fig. 3(a). Because the sizes of the capacitors C_{C1} and C_{C2} are comparable to the source capacitance of the piezoelectric transducer, they have been implemented off-chip. The transistor sizes of M_{C1} and M_{C2} were chosen to be $\frac{15\ \mu m}{6\ \mu m}$. To avoid the parasitic p-n-p transistor formed by the p-n diode with p-substrate, D_1-D_6 and D_7-D_{13} are realized using PMOS transistor whose bulk voltage is interpolated by a circuit similar to a configuration formed by P_2 and P_3.

A unity-gain buffer with DC open-loop gain larger than 75 dB is used for reading out the voltage on the floating-gate node as shown in Fig. 4. To prevent the floating-gate charge from leaking to the oxide through the vias, the FG node is formed using the first polysilicon layer and is connected to the input of the amplifier through the same poly layer. To avoid hot-electron injection through the gate of the input transistors of the read-out amplifier, the voltage of the FG is maintained below 3.4 V during readout phase. Also, when the injector is self-powered through the energy transducer, the power to the read-out buffer is disabled.

B. Measurement Results

The injector was prototyped in a standard 0.5-μm CMOS process using circuit components whose form factors are summarized in the table I. The micrograph of the fabricated prototype is shown in Fig. 5 and the injector circuit occupies an area of 200 μm $\times$ 150 μm.

The first group of experiments was designed to verify the dynamic response of the compensation circuit. A signal generator was used for generating a periodic ramp signal with different rise-times and at a duty-cycle of 10% and the signal is directly applied to the input of the injector. For this experiment, the circuit in Fig. 4 was configured in a single-ended mode

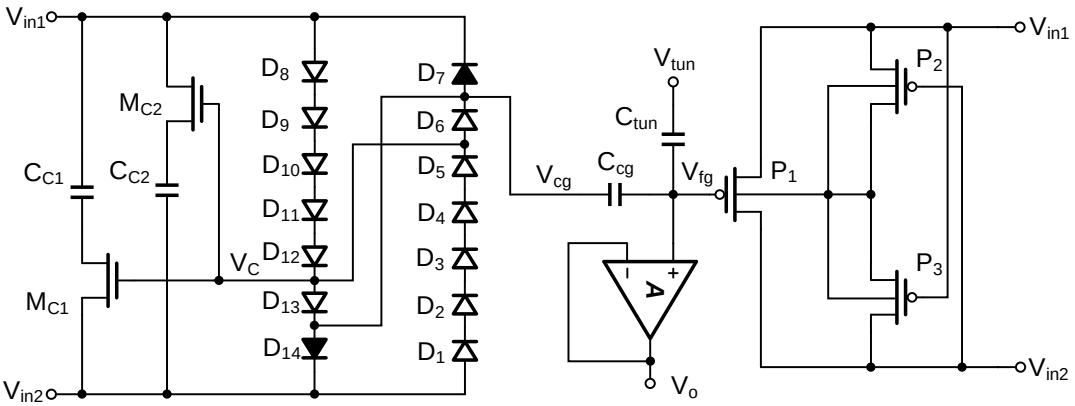

Fig. 4. Circuit schematic of a complete fully-differential p-IHEI injector with a fully differential compensation module.

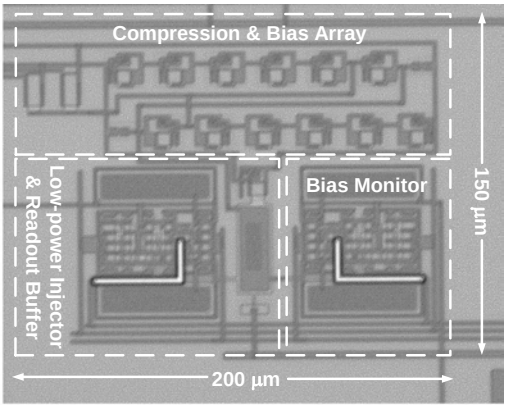

Fig. 5. Micro-photograph of the fabricated prototype.

TABLE I. SPECIFICATIONS OF THE PROTOTYPED CIRCUIT

Parameter	Value
Technology	0.5-μm CMOS
Die Size	1.5 $\times$ 1.5 mm^2
Layout Size	200 $\times$ 150 μm^2
Minimum Current	$<$ 1 nA
Diode Current	$<$ 0.2 nA
Power range	5 nW $\sim$ 1.5 μW

with one of the input terminals connected to ground. The compression capacitor C_C is chosen as 10 nF. Fig. 6(a) shows the measured V_D when the input rate is set to 50 V/s. The measured response show that as the input signal ramps up, the transistor M_{C1} turns ON. As a result, the pull-down current through the transistor is larger than the displacement current flowing through the capacitor (which is a function of the signal ramp-rate). As a result, the capacitor is fully engaged which will result in the response illustrated in phase III in Fig. 3. However, when the ramp-rate is increased, as shown in Fig. 6(b)-(d), V_D is able to track V_L implying the capacitor is initially disengaged (unconnected) before being connected to the network. Thus, the dynamic response of the compensation circuit will be able to dynamically interpolate between the phases I and III of the desired response. This dynamic response will be a function of the capacitance C_{C1} and the gate voltage of M_{C1} which is determined by the diode network in Fig. 4.

The second experiment was designed to verify the compressive response of the compensation circuit. For this setup the piezoelectric transducer was emulated using a current source I_p parallel with a source capacitor C_p as illustrated in Fig. 7. C_p was chosen to be 1 μF, and C_C was chosen to be 2 μF. The load resistor R_L was set to be 10 MΩ. A Keithley 2400 source-meter was used to generate 5 μA, 10 μA, 20 μA, and 40 μA of current as shown in Fig. 8(a), (b), (c), and (d) respectively. The measured response, shown in Fig. 8(a), can be explained using four temporal phases. In phase 1, V_D follows the change in V_L because the capacitor C_C is disengaged. During this stage, most of the power is consumed by the load R_L. In phase 2, the transistor M_1 starts drawing current and most of the source current is used to charge the energy storage capacitor C_C. As a result V_L starts to show a compressive response. When M_1 is completely on, the circuits enter into stage 3, namely the compensation mode, the capacitor C_C is fully engaged. During the last stage, current source is turned OFF and the energy stored in the capacitor C_p and C_C is discharged through the load R_L. Similar to the previous experiment, the dynamic response of the compensation circuit are verified for different magnitudes of the source current. The results also imply that with large input power, large $C_{Ci}(i = 1, 2)$ is required for effective compression.

The next set of experiments verified the operation of the injector under three different source models: constant current source, constant voltage source and constant power source. A Keitheley 2400 source meter was used to bias the injector in different modes. In constant current mode, a current source was applied directly to the injector in Fig. 3(b). Fig 9 shows the measured response of the injector. Because the floating gate voltage V_{fg} decreases, the source voltage will also decrease implying a slower injection rate. Therefore, constant current

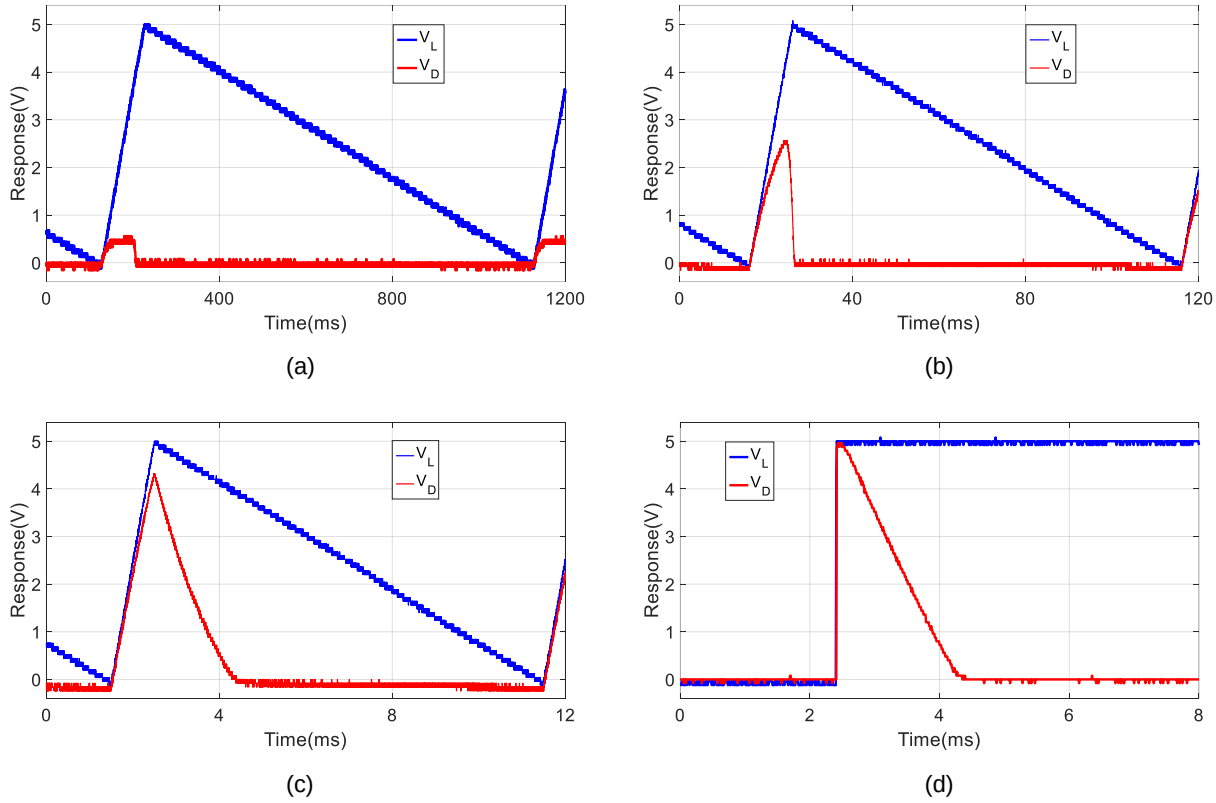

Fig. 6. Measured response of the compensation circuit for different signal-rates: (a) 50 V/s, (b) 500 V/s, (c) 5000 V/s, and (d) pulse stimulus.

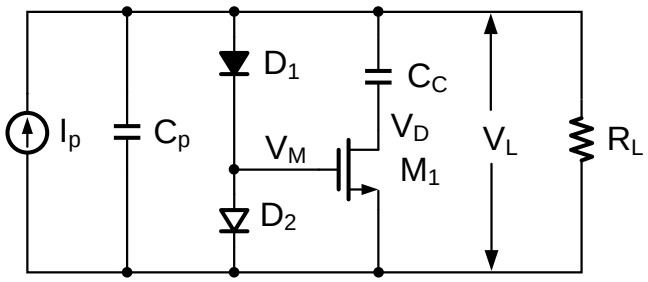

Fig. 7. Schematic of the test setup used for verifying the compressive response of the compensation circuit.

injection demonstrates a saturation behavior as shown in Fig. 9.

In contrast, for constant voltage mode, where the source-to-drain voltage of transistor M_2 in Fig. 3 is kept constant, the injection rate will first increase because the source current increases, as shown by equation 3. However, when the current is large, the overdrive voltage dropped in the pinch-off region decreases which implies the energy of hot electrons will decrease at the same time. When this negative effect overcomes the positive feedback brought by the increasing channel current, the injection speed starts to decrease. This saturation process is also illustrated by the measured results shown in Fig. 10.

In constant power mode, we used the Keitheley source meter to periodically update the voltage and current to ensure the input power to the injector is constant. The measured responses with constant input power from 5 nW to 15 nW are shown in Fig. 11, which shows a quasi-linear response. The constant-power operation of the proposed hot-electron injector can be understood intuitively based on the following two observations: (a) constant current mode hot-electron injection is a negative-feedback process and $V_{fg}(t)$ shows a saturating response as shown in Fig. 9; and (b) constant voltage mode hot-electron injection is a positive-feedback process where $V_{fg}(t)$ decreases exponentially as shown in Fig. 10. Thus, when the input power is constrained to be constant (or product of input voltage and input current is constant) the hot-electron injection should interpolate between both the negative and positive feedback process, leading to a quasi-linear response. The measured results of the injector are consistent with the conclusions in [13].

For the fourth set of experiments the functionality of the proposed injector was validated by interfacing with a miniature commercial off-the-shelf (COTS) piezoelectric transducer (dimensions: 10mm×5mm×0.1mm, material: PZT-5H) operating in a strain-mode. Since the response of the piezoelectric

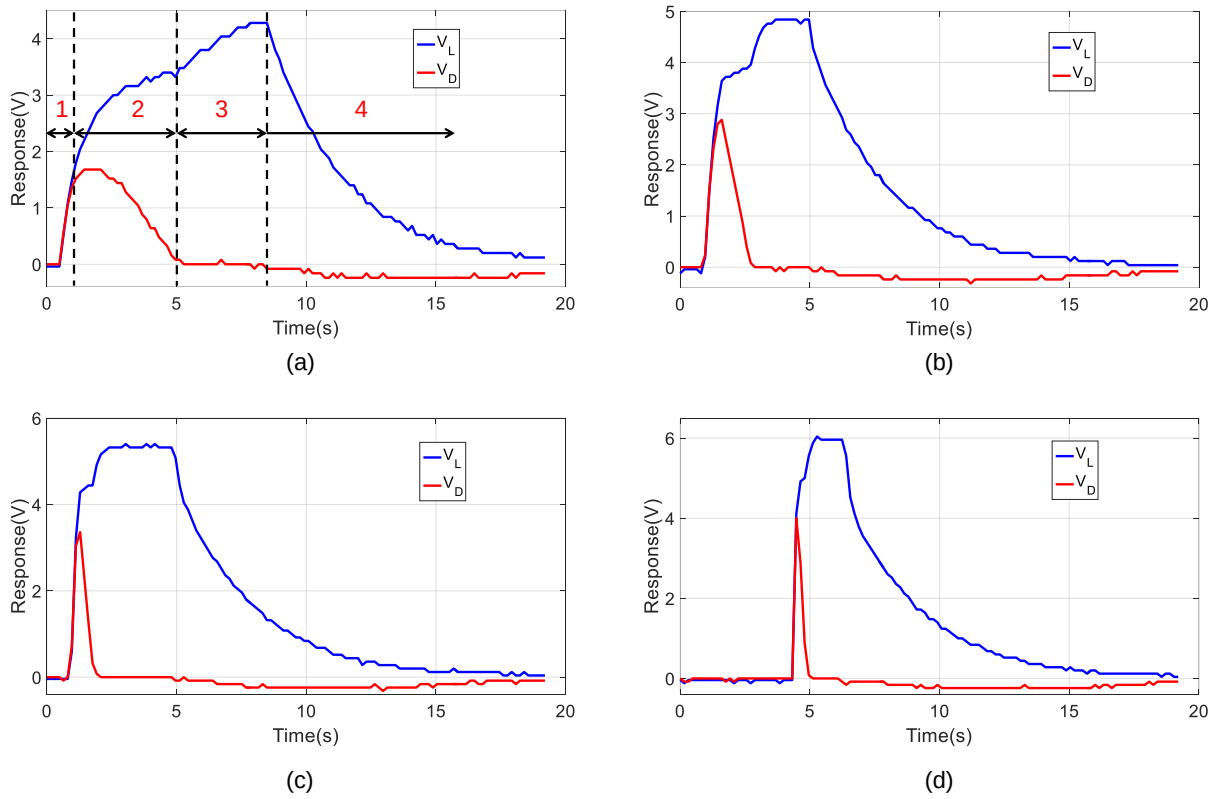

Fig. 8. Measured response of the compensation circuit for different magnitudes of source currents : (a) 5 μA, (b) 10 μA, (c) 20 μA, and (d) 40 μA.

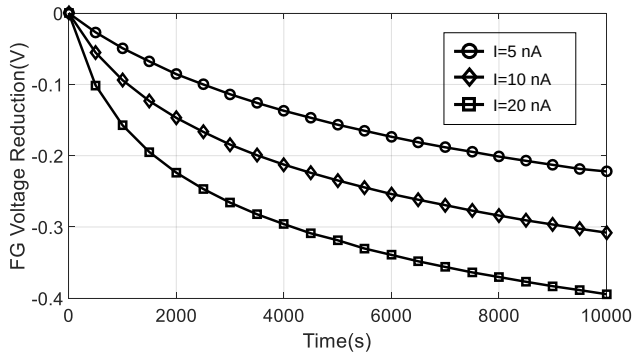

Fig. 9. Measured injector response when driven by a constant current source.

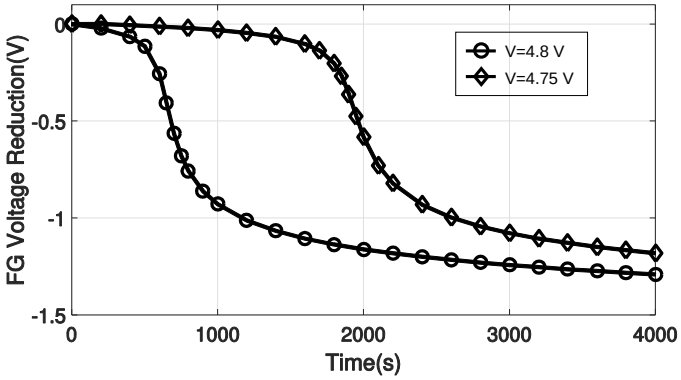

Fig. 10. Measured injector response when driven by a constant voltage source.

transducer have already been verified in our previous papers using different biomedical phantoms [13] (as shown in the inset of Fig. 14), we have emulated the response using a benchtop set up which can be configured to generate different levels of input power. Note that due to the diversity of applications that the proposed injector could be applied to (shown in Fig. 1), a controlled phantom / test-bed experiment seemed more appropriate. This way we are be able to verify the response of the sensor while avoiding issues related with packaging and sensor attachment with different biomechanical structures, like bone, stents and wearables. For the benchtop experiments, the transducer was subject to periodic mechanical excitation (step displacement) such that it generated different levels of output power. To measure the power delivered by the transducer, a resistive load was connected to the output of the cantilever. For a specific mechanical excitation pattern,

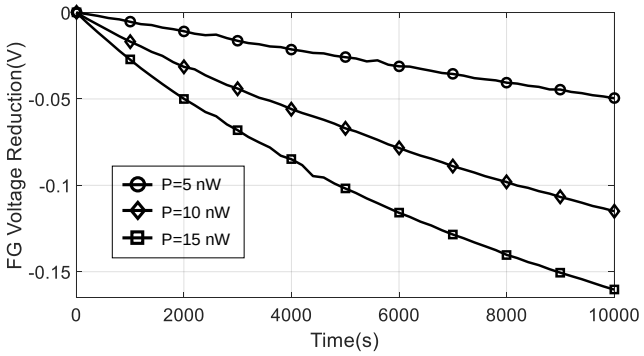

Fig. 11. Measured injector response when driven by a constant power source.

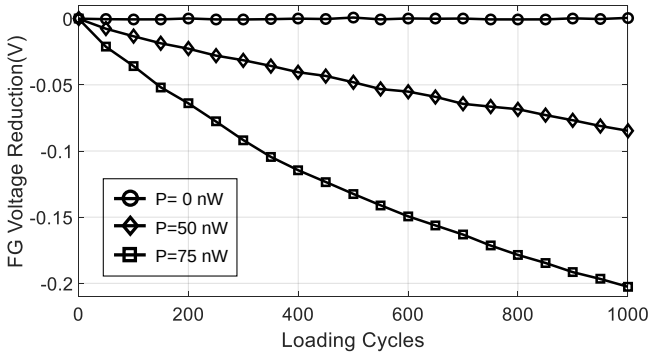

Fig. 12. Measured injector responses for different magnitude of input power ($C_{TD} = 1.5nF$).

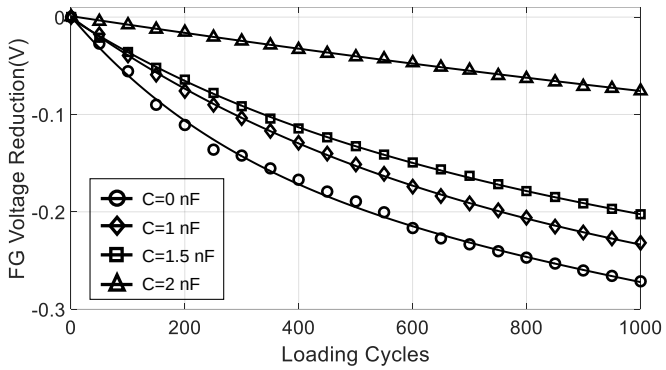

Fig. 13. Measured injector responses for different values of compensation capacitances (P_{in}=75 nW).

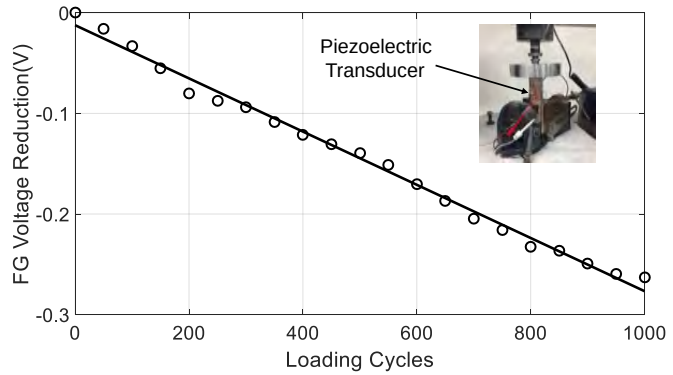

Fig. 14. Measured injector responses when the p-IHEI sensor is directly driven by a ceramic PZT-5H transducer for C_C=100 nF and average input power P_{in}=1500 nW. The benchtop setup emulates the biomechanical phantom shown in the inset which was reported in our previous work [13]

the voltage was measured across the resistive load which was then used to determine the output power level. The resistor was then replaced by the fabricated injector and the transducer was again subjected to similar mechanical excitation. A pair of off-chip capacitors with 1.5 nF capacitance were connected as the compressive capacitor. The injectors' response to the cantilever with different input power levels are shown in Fig. 12, which validate the quasi-linear response.

The next set of experiments were designed to determine the effect of compensation circuit parameters on the linearization of the proposed injector. Different compensation capacitances with values ranging from 0 nF to 2 nF were used and the measured responses are shown in Fig. 13. $C_C = 0$ equals to the case that there is no compensation circuit and the circuit degenerates to the case described in [13]. With the increase of capacitance, the charge injected to the FG node is decreased due to the compressive response of the compensation circuit. As a result, the linearity of the injector is improved validating the functionality of the compensation circuit.

The last experiment was designed to verify that the proposed injector could be adapted to different applications with different input power by adjusting the magnitude of the compensation capacitor. A ceramic piezoelectric transducer (Outer diameter: 20 mm, inner diameter:15 mm, material: PZT) was integrated with the injector to generate larger power output. The compression capacitor was chosen as 100 nF to accommodate power ranging from 1 μW to 2 μW. The piezoelectric transducer was subject to periodic mechanical excitations. The floating gate voltage was initialized to 3.4 V and injector's response was measured and recorded as shown in Fig. 14, which displays an almost linear dependence with respect to the number of mechanical loading cycles.

Fig. 15 summarizes the response of the linearized injectors for different input power levels which also includes the error residue estimated after a linear regression over the measured data. The linearity of the injection results can be estimated by the ratio between the injection range and the largest regression error, and the measured results show that the proposed method can achieve a linearity of more than 25 dB, which is significantly better than [13]. Note that in [7] we had reported a linear injector with more than 40dB linear range; however, the injector could only be activated at power levels greater than 100nW. This design therefore represents a significant improvement over the prior work. Also note that the linearity of the proposed injector can be further improved by choosing

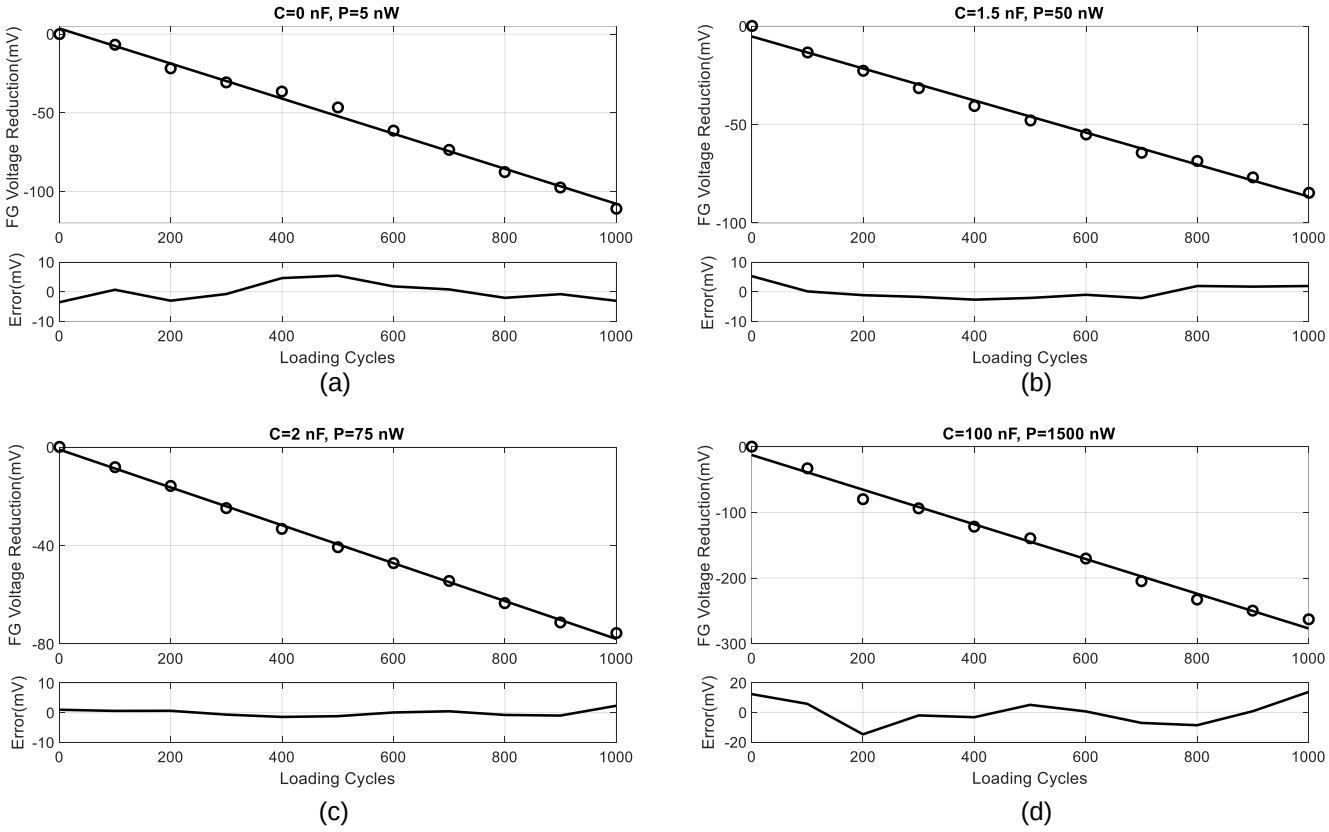

Fig. 15. Linearization of the injector response for different levels of input power by choosing different values of the compensation capacitances.

a larger value of the compensation capacitance, however at the expense of lower sensitivity. For instance, when the input power is reduced to as low as 5 nW, the injector shows a linear response without any compensation. However, when the input power level was increased the compensation circuit requires a larger capacitance for linearization. As an example, a 2 nF capacitor is sufficient to achieve a linearity of 25dB for an average input power of 75 nW applied over a duration of 1000 loading cycles. When the input power is increased to 1500 nW, the capacitance had to be increased to 100 nF. In principle the compensation circuit should be able to linearize the response of the injector beyond 1500 nW by appropriately choosing a larger value of the capacitance. Table II summarizes a prescription of a minimum value of the compensation capacitor that needs to be chosen to linearize the response of the injector. Note that a larger compensation capacitance would enhance the linearity of the injector, however, the sensitivity of the measurement will also reduce, as was demonstrated in Fig. 13. Conversely, for compensation capacitances greater than the minimum value shown in Table II, the linearity would be enhanced for power levels lower than what is specified in Table II. This implies that the value of the compensation capacitor is a design parameter that needs to be chosen based on the target application and the size and material properties of the piezoelectric transducer, as shown in Fig. 1. Also shown in Table II is the extrapolated minimum value of compensation capacitor required to linearize the injector at mW of input power. Thus, the proposed injector could potentially replace the linear injector that was previously used for self-powered monitoring of head-impacts in helmeted sports [11].

TABLE II. MINIMUM COMPENSATION CAPACITANCE FOR LINEARIZATION

Power	Capacitance
5 nW	0 nF
50 nW	1.5 nF
75 nW	2 nF
1.5 μW	100 nF
1 mW	100 μF(extrapolated)

IV. CONCLUSIONS

In this paper, we proposed an improvement to our previously reported ultra-low power CMOS hot-electron injector by linearizing its response to different magnitudes of input power. As a result the proposed injector can be used in a variety of applications that require continuous and implanted monitoring of biomechanical strain. For each application and for each input power range, the magnitude of the compensation capacitor needs to be chosen to be larger than a minimum experimentally determined value, to achieve the target linear

response. Future work in this area will focus on adaptively choosing the value of the compensation capacitor based on historical statistics or by using a well defined deployment protocol.

REFERENCES

[1] L. Schwiebert, S. K. Gupta, and J. Weinmann, "Research challenges in wireless networks of biomedical sensors," in *Proceedings of the 7th annual international conference on Mobile computing and networking*. ACM, 2001, pp. 151–165.

[2] S. R. Platt, S. Farritor, K. Garvin, and H. Haider, "The use of piezoelectric ceramics for electric power generation within orthopedic implants," *Mechatronics, IEEE/ASME Transactions on*, vol. 10, no. 4, pp. 455–461, 2005.

[3] N. G. Elvin, N. Lajnef, and A. A. Elvin, "Feasibility of structural monitoring with vibration powered sensors," *Smart materials and structures*, vol. 15, no. 4, p. 977, 2006.

[4] E. Romero, R. Warrington, and M. Neuman, "Energy scavenging sources for biomedical sensors," *Physiological measurement*, vol. 30, no. 9, p. R35, 2009.

[5] N. Lajnef, N. G. Elvin, and S. Chakrabartty, "A piezo-powered floating-gate sensor array for long-term fatigue monitoring in biomechanical implants," *Biomedical Circuits and Systems, IEEE Transactions on*, vol. 2, no. 3, pp. 164–172, 2008.

[6] C. Huang, N. Lajnef, and S. Chakrabartty, "Calibration and characterization of self-powered floating-gate usage monitor with single electron per second operational limit," *Circuits and Systems I: Regular Papers, IEEE Transactions on*, vol. 57, no. 3, pp. 556–567, 2010.

[7] C. Huang, P. Sarkar, and S. Chakrabartty, "Rail-to-rail, linear hot-electron injection programming of floating-gate voltage bias generators at 13-bit resolution," *Solid-State Circuits, IEEE Journal of*, vol. 46, no. 11, pp. 2685–2692, 2011.

[8] C. Huang and S. Chakrabartty, "An asynchronous analog self-powered cmos sensor-data-logger with a 13.56 mhz rf programming interface," *Solid-State Circuits, IEEE Journal of*, vol. 47, no. 2, pp. 476–489, 2012.

[9] B. Fang, T. Feng, M. Zhang, and S. Chakrabartty, "Feasibility of b-mode diagnostic ultrasonic energy transfer and telemetry to a cm 2 sized deep-tissue implant," in *Circuits and Systems (ISCAS), 2015 IEEE International Symposium on*. IEEE, 2015, pp. 782–785.

[10] Y. Alazzawi, C. Qian, and S. Chakrabartty, "Feasibility of non-contact ultrasound generation using implanted metallic surfaces as electromagnetic acoustic transducers," in *Biomedical Circuits and Systems Conference (BioCAS), 2015 IEEE*. IEEE, 2015, pp. 1–4.

[11] T. Feng, K. Aono, T. Covassin, and S. Chakrabartty, "Self-powered monitoring of repeated head impacts using time-dilation energy measurement circuit," *Biomedical Circuits and Systems, IEEE Transactions on*, vol. 9, no. 2, pp. 217–226, 2015.

[12] A. dos Santos, W. Yaegashi, R. Marcon, B. Li, R. Gelamo, L. Cardoso, J. Sasaki, M. Miranda, and F. Mello, "Rochelle salt piezoelectric coefficients obtained by x-ray multiple diffraction," *Journal of Physics: Condensed Matter*, vol. 13, no. 46, p. 10497, 2001.

[13] L. Zhou, A. C. Abraham, S. Y. Tang, and S. Chakrabartty, "A 5nw quasi-linear cmos hot-electron injector for self-powered monitoring of biomechanical strain variations," *Biomedical Circuits and Systems, IEEE Transactions on*, 2016.

[14] W. Borchani, K. Aono, N. Lajnef, and S. Chakrabartty, "Monitoring of post-operative bone healing using smart trauma-fixation device with integrated self-powered piezo-floating-gate sensors," *Biomedical Engineering, IEEE Transactions on*, 2015.

[15] S. Chakrabartty and N. Lajnef, "Infrasonic power-harvesting and nanowatt self-powered sensors," in *Circuits and Systems, 2009. ISCAS 2009. IEEE International Symposium on*. IEEE, 2009, pp. 157–160.

[16] P. E. Hasler, "Foundations of learning in analog vlsi," Ph.D. dissertation, California Institute of Technology, 1997.

[17] E. Vittoz and J. Fellrath, "Cmos analog integrated circuits based on weak inversion operations," *Solid-State Circuits, IEEE Journal of*, vol. 12, no. 3, pp. 224–231, 1977.

Liang Zhou (SM'14)received the B.S. degree in physics from Tsinghua University, Beijing, China, in 2010. Currently, he is working toward the Ph.D. degree in the Department of Computer Science and Engineering, Washington University, St. Louis, MO, USA. His research interests include low-power sensing systems, integrated biomedical sensors, analog and mixed-signal circuits, and RF circuits.

Shantanu Chakrabartty (SM'99-M'04-S'09) received his B.Tech degree from Indian Institute of Technology, Delhi in 1996, M.S and Ph.D in Electrical Engineering from Johns Hopkins University, Baltimore, MD in 2002 and 2004 respectively. He is currently a professor in the School of Applied Sciences and Engineering at Washington University in St. Louis. From 2004-2015, he was an associate professor in the department of electrical and computer engineering at Michigan State University (MSU). From 1996-1999 he was with Qualcomm Incorporated, San Diego and during 2002 he was a visiting researcher at The University of Tokyo. Dr. Chakrabartty's work covers different aspects of analog computing, in particular non-volatile circuits, and his current research interests include energy harvesting sensors and neuromorphic and hybrid circuits and systems. Dr. Chakrabartty was a Catalyst foundation fellow from 1999-2004 and is a recipient of National Science Foundation's CAREER award, University Teacher-Scholar Award from MSU and the 2012 Technology of the Year Award from MSU Technologies. Dr. Chakrabartty is a senior member of the IEEE and is currently serving as the associate editor for IEEE Transactions of Biomedical Circuits and Systems, associate editor for the Advances in Artificial Neural Systems journal and a review editor for Frontiers of Neuromorphic Engineering journal.